

Double ionization of helium by proton impact: A generalized-Sturmian approachM. J. Ambrosio,^{1,2,*} D. M. Mitnik,^{1,2} L. U. Ancarani,³ G. Gasaneo,^{2,4} and E. L. Gaggioli⁴¹*Instituto de Astronomía y Física del Espacio (IAFE, CONICET-UBA), Casilla de Correo 67 - Sucursal 28 (C1428ZAA), Ciudad Autónoma de Buenos Aires, Argentina*²*Consejo Nacional de Investigaciones Científicas y Técnicas, Buenos Aires, Argentina*³*Théorie, Modélisation, Simulation, SRSMC, UMR CNRS 7565, Université de Lorraine, 57078 Metz, France*⁴*Departamento de Física, Universidad Nacional del Sur, 8000 Bahía Blanca, Buenos Aires, Argentina*

(Received 1 September 2015; published xxxxx)

We present *ab initio* calculations for the double ionization of helium by fast proton impact, using the generalized-Sturmian-functions methodology and within a perturbative treatment of the projectile-target interaction. The cross-section information is extracted from the asymptotic behavior of the numerical three-body function that describes the emission process. Our goal is to provide benchmark first-order Born fully differential cross sections with which one may investigate the suitability of transition matrices calculated using approximate analytic-type solutions for the double continuum (the choice of effective charges or effective momenta to partially account for the internal target interactions being, to some extent, arbitrary). We also provide fully differential cross sections for the low-ejection-energy regime, which is beyond the suitable range of such perturbative methods. We find, however, that the effective momentum approach allows one to get at least a rough characterization of the most dominant physical process involved. We also compare our calculations with the only available relative experimental set, showing an agreement in shape that can be well understood within the given momentum transfer regime.

DOI: [10.1103/PhysRevA.00.002700](https://doi.org/10.1103/PhysRevA.00.002700)

PACS number(s): 34.50.Fa, 31.15.A–

I. INTRODUCTION

The double ionization of helium by charged-particle impact constitutes an intricate four-body Coulomb problem, appreciably more complex than in the case of impact by photons. This is due to the, in principle, two-center interaction between the projectile and the target. If the projectile is positively charged, the collision can lead to the capture of one of the target electrons and the ionization of the other one. However, this process is several orders of magnitude less probable than ordinary single or double ionization (DI), particularly for projectiles on the order of 1–10 MeV/amu [1]. In this contribution we focus on proton-impact ionization of helium within the high-incident-energy regime for which the capture process can be disregarded. The most basic mechanisms which produce DI, called shake-off (SO), two-step-1 (TS1) and two-step-2 (TS2) [2], were studied with approximate descriptions of both the helium ground state and the double continuum [3,4]. The TS1 process implies a collision between the projectile and one of the target electrons, which subsequently impacts the other one, and both end up being ejected to the continuum. In the TS2 mechanism, the projectile hits the two target electrons successively and kicks them out of their parent core. Another mechanism, called two-step-1-elastic (TS1EL) in Ref. [3], contemplates a further collision between the projectile and the electron ejected via the electron-electron interaction after the first impact. Processes TS2 and TS1EL require two projectile-target Born interactions.

The majority of previous works, both theoretical and experimental, discussed integrated cross sections [5–10]. To a lesser extent, fully differential cross sections (FDCS),

which provide the most detailed information of the double-ionization process, have also been investigated experimentally and theoretically [3,4,11,12]. For the case of electron impact several FDCS measurements under different emission energies and momentum transfer regimes have been carried out by the Orsay and Heidelberg groups (restricted to fast projectiles; see Refs. [13–16]); many theoretical studies have been dedicated to interpreting these data (a nonexhaustive list of references is given in the introduction of our most recent publications [17,18] on the topic). In comparison, much less frequent are differential cross-section measurements for proton impact. The one reported by Fischer *et al.* [11] is the only experimental data set that provides a fully differential cross section, while previous works [5–8] have measured total cross sections and double-to-single ionization ratios. In Ref. [11], the authors report that one week was required to observe 200 000 double-ionization events, enough to produce FDCS. A set of multiply, but not fully, differential cross-section measurements, along with their theoretical counterparts, was published in Ref. [3] for double ionization of helium by very fast (6 MeV) protons, in addition to a comparison of their calculations with one of the kinematic configurations from Ref. [11].

On the theoretical side, the collision of charged projectiles with helium atoms constitutes a full four-body problem which poses a formidable challenge. If the projectile is fast enough, its interaction with the target can be considered a perturbation, with the projectile experiencing a single deflection. While the resulting three-body problem is still challenging enough, there exists nowadays a variety of numerical schemes that can solve it from first principles in a time-dependent [9,10] or time-independent fashion [19–22]. Other approaches use approximate analytical three-body functions, mostly based on the 3C (also named C3 or BBK) wave function [23,24] which is asymptotically correct when all three particles are far from each other. Quite a number of variants of the 3C function have

*Corresponding author: mj_ambrosio@iafe.uba.ar

88 been proposed in the literature; they all aim to improve the
 89 3C function by including extra physical information, thereby
 90 extending its range of validity. One way to achieve this is
 91 by introducing effective charges which, although with some
 92 restrictions, are largely arbitrary. Effective charges allow one
 93 to better account for intratarget interactions as well as projectile-
 94 target ones beyond the first Born approximation (FBA). The
 95 comparison of calculated cross sections, in particular FDCS,
 96 with either experimental or benchmark *ab initio* theoretical
 97 data then provides an instrument to point out which set is more
 98 physically sound for given kinematical conditions. While such
 99 approximate analytical three-body functions generally provide
 100 only qualitative descriptions, they are often good enough to
 101 analyze and identify the dominant collisional mechanisms.
 102 Fully numerical approaches, in turn, provide, in principle,
 103 exact solutions, but the interpretation of the resulting cross
 104 sections is less straightforward. One has to infer which
 105 mechanics come into play just by analyzing the cross sections.

106 For the double ionization of helium by electron impact,
 107 thorough comparisons between theoretical and experimental
 108 FDCS, on the one hand, and between fully numerical and
 109 approximate analytical calculations, on the other hand, have
 110 been presented in the literature (see, e.g., the recent studies
 111 in Refs. [17,18] and references therein). In contrast, very little
 112 has been done for proton impact. This paper aims to contribute
 113 to filling that gap.

114 We calculate FDCS with a Sturmian approach based on
 115 generalized Sturmian functions (GSF) [22,25]. The spectral
 116 method has been shown to deal successfully with three-body
 117 scattering problems, as illustrated recently through the study
 118 of the double ionization of helium by photons [26] or by
 119 fast electrons [17,18]. The GSF method can generate both
 120 the target bound state and its scattering function with, in
 121 principle, arbitrary numerical accuracy. Here, we apply it
 122 to study the fast proton-helium double-ionization process: in
 123 chosen kinematical conditions we provide, within the FBA,
 124 benchmark FDCS with three goals in mind. First, we want
 125 to compare our FDCS with those presented in the recent
 126 theoretical investigations based on perturbative methods using
 127 approximate analytical three-body wave functions [4,12].
 128 Second, we wish to identify the collisional processes and
 129 contrast them with those of the better-known electron-impact
 130 counterpart. Third, we want to find out if a fully numerical
 131 treatment within the FBA is able to reproduce the main features
 132 observed in the experiments reported in [11].

133 López *et al.* [12] made a thorough investigation of fast
 134 proton-helium FDCS under a variety of kinematical condi-
 135 tions. They demonstrated a great degree of variation in
 136 the calculated cross sections when using different analytical
 137 final-state continuum functions (3C and variants including
 138 effective charges). They also showed that the target bound-state
 139 description affects the FDCS palpably. The same authors fur-
 140 ther tackled the problem with an approach involving effective
 141 momenta [4]. In this second study, the obtained cross sections
 142 present structures that vary slowly with the ejection angles, a
 143 trend, to some degree, analogous to that observed for electron
 144 impact [16,18,27]. By providing FDCS with our GSF method,
 145 we wish to evaluate the success of these perturbative schemes.

146 Recall that the 3C continuum function is valid when the
 147 particles are moving away from each other quickly and/or

are far apart. There is therefore a particular niche for which
 the perturbative methods are not well suited: low emission
 energies. To explore this regime, we have performed GSF
 calculations considering a total excess energy of 6 eV, with the
 equal-energy-sharing case, (3 + 3) eV, as well as the unequal
 configuration, (1.5 + 4.5) eV. The purpose here is twofold.
 First, we explore these kinematical conditions with a reliable
 method to establish the physical processes that come into play
 when the two electrons are emitted very slowly. Second, our
 benchmark results can be used to test the quality of effective
 charges intended to extend the validity of the 3C function
 to the low-energy domain. By no means do we intend to
 disqualify the perturbative approaches. On the contrary, we
 regard them as complementary to *ab initio* methods, each
 exploring adequately different kinematical ranges.

163 Since there is a lot of variation, even within the first-order
 164 Born model, from one perturbative model to the next, we are
 165 not considering in the present work any second-order Born
 166 interactions of the projectile with the target atom. An interested
 167 reader can find second-order studies in Refs. [3,28,29]. For
 168 this contribution we consider it a priority to establish first
 169 the first-order Born ground properly. To this order, valid
 170 for fast projectiles, the phenomenon of electronic capture
 171 is not incorporated in the calculations, either numerical or
 172 perturbative. Thus, only the effects of the well-known two-
 173 step-1 and shake-off mechanisms are expected to be observed
 174 in the calculated FDCS.

175 The rest of the paper is arranged as follows. In Sec. II we
 176 begin by outlining the theoretical framework on which our
 177 calculations are based. Section III, dedicated to the results,
 178 is divided in three subsections. The first one is devoted to a
 179 comparison of the GSF results with those obtained with the
 180 effective charges and effective momenta approaches [4,12].
 181 Section III B contains the studies performed in the low-
 182 emission regimes (6 eV excess energy): we make a comparison
 183 with a preexisting result [4] in equal energy sharing; we then
 184 increase the momentum transfer to observe more prominent
 185 nondipolar effects. In Sec. III C we contrast our numerical
 186 calculations with the experimental data reported in [11].
 187 Finally, a brief summary is provided in Sec. IV.

188 Atomic units ($\hbar = e = m_e = 1$) are used throughout the
 189 article, unless otherwise stated.

190 II. FAST PROJECTILE FORMULATION AND GSF 191 APPROACH

192 Our treatment of the four-body scattering problem is based
 193 on a perturbative series of the projectile-target interaction, kept
 194 up to the first order. The resulting three-body problem is then
 195 solved with the GSF method.

196 Let \mathbf{r}_1 denote the position of the projectile (mass m_P), \mathbf{r}_i
 197 ($i = 2,3$) denote that of the two helium electrons with respect
 198 to its nucleus (mass m_T , charge $Z = 2$), and $r_{ij} = |\mathbf{r}_i - \mathbf{r}_j|$
 199 denote the distance between particles i and j . The full four-
 200 body Hamiltonian reads

$$\begin{aligned}
 H = & -\frac{1}{2\mu_{TP}} \nabla_1^2 - \frac{1}{2\mu_T} \nabla_2^2 - \frac{1}{2\mu_T} \nabla_3^2 + \frac{Z}{r_1} - \frac{1}{r_{12}} \\
 & - \frac{1}{r_{13}} - \frac{Z}{r_2} - \frac{Z}{r_3} + \frac{1}{r_{23}}, \quad (1)
 \end{aligned}$$

with the reduced masses defined as $\mu_{TP} = \frac{m_p m_T}{m_p + m_T}$ and $\mu_T = \frac{m_T}{m_T + 1}$. Similar to Refs. [18,30], we write subsequently

$$H_0 = h_p + h_{He}, \quad (2)$$

where

$$h_{He} = \left(-\frac{1}{2\mu_T} \nabla_2^2 - \frac{1}{2\mu_T} \nabla_3^2 - \frac{Z}{r_2} - \frac{Z}{r_3} + \frac{1}{r_{23}} \right) \quad (3)$$

is the three-body helium Hamiltonian and $h_p = -\frac{1}{2\mu_{TP}} \nabla_1^2$ is the free-particle kinetic term associated with the projectile. The two Hamiltonians in (2) act separately on the subsystem (2,3) and (1). They are coupled through the perturbation

$$\bar{W} = \frac{Z}{r_1} - \frac{1}{r_{12}} - \frac{1}{r_{13}}. \quad (4)$$

The four-body Hamiltonian is then

$$H = H_0 + \bar{W}, \quad (5)$$

and the Schrödinger equation with outgoing-type (+) behavior reads

$$[H_0 + \bar{W} - E] \Psi^+(\mathbf{r}_1, \mathbf{r}_2, \mathbf{r}_3) = 0, \quad (6)$$

where E is the total energy.

As shown in Ref. [30], the Schrödinger equation (6) can be transformed into a system of coupled differential equations if the solution is proposed as

$$\Psi^+(\mathbf{r}_1, \mathbf{r}_2, \mathbf{r}_3) = \sum_n \Psi^{(n)+}(\mathbf{r}_1, \mathbf{r}_2, \mathbf{r}_3), \quad (7)$$

where each order retains n interactions \bar{W} between the projectile and the target. Allowing for only one interaction, we need the zeroth- and first-order expressions, which read

$$[H_0 - E] \Psi^{(0)+}(\mathbf{r}_1, \mathbf{r}_2, \mathbf{r}_3) = 0, \quad (8a)$$

$$[H_0 - E] \Psi^{(1)+}(\mathbf{r}_1, \mathbf{r}_2, \mathbf{r}_3) = -\bar{W} \Psi^{(0)+}(\mathbf{r}_1, \mathbf{r}_2, \mathbf{r}_3). \quad (8b)$$

The zeroth order corresponds to a separable solution, $e^{i\mathbf{k}_i \cdot \mathbf{r}_1} \Phi_i(\mathbf{r}_2, \mathbf{r}_3)$, where $\Phi_i(\mathbf{r}_2, \mathbf{r}_3)$ is the two-electron helium ground state and the fast incident projectile is described by a plane wave of momentum \mathbf{k}_i . The first-order solution, verifying Eq. (8b), is written as [30]

$$\Psi^{(1)+}(\mathbf{r}_1, \mathbf{r}_2, \mathbf{r}_3) = \frac{1}{(2\pi)^{3/2}} \int d\mathbf{k} e^{i\mathbf{k} \cdot \mathbf{r}_1} \Phi_{sc}^+(\mathbf{k}, \mathbf{r}_2, \mathbf{r}_3), \quad (9)$$

where the three-body scattering (labeled sc) function Φ_{sc}^+ characterizes the physics of the ejected electrons. Let E_a denote the energy of two electrons interacting with the nucleus in the final state and $k^2/2$ be the energy associated with the projectile: the total energy of the system is then $E = E_a + k^2/(2\mu_{TP})$. Let the projectile be scattered with momentum \mathbf{k}_f , and define the momentum transfer vector $\mathbf{q} = \mathbf{k}_i - \mathbf{k}_f$. Inserting Eq. (9) into (8b), we obtain a driven equation for $\Phi_{sc}^+(\mathbf{q}, \mathbf{r}_2, \mathbf{r}_3)$ [30]:

$$[h_{He} - E_a] \Phi_{sc}^+(\mathbf{q}, \mathbf{r}_2, \mathbf{r}_3) = -\frac{4\pi}{q^2} \frac{1}{(2\pi)^3} (Z - e^{i\mathbf{q} \cdot \mathbf{r}_2} - e^{i\mathbf{q} \cdot \mathbf{r}_3}) \times \Phi_i(\mathbf{r}_2, \mathbf{r}_3), \quad (10)$$

where we have made explicit the \mathbf{q} dependence in the three-body scattering wave function.

Formally, we can write the asymptotic behavior of $\Phi_{sc}^+(\mathbf{q}, \mathbf{r}_2, \mathbf{r}_3)$ as [31]

$$\Phi_{sc}^+(\mathbf{q}, \mathbf{r}_2, \mathbf{r}_3) \xrightarrow{\rho \rightarrow \infty} (2\pi i)^{1/2} \kappa^{\frac{3}{2}} T_{\tilde{\mathbf{k}}_2, \tilde{\mathbf{k}}_3} \frac{e^{i[\kappa\rho - \lambda_0 \ln(2\kappa\rho) - \sigma_0]}}{\rho^{\frac{5}{2}}}, \quad (11)$$

where $\rho = \sqrt{r_2^2 + r_3^2}$ is the hyperradius, $\kappa = \sqrt{2E_a}$ the hypermomentum, σ_0 is a Coulomb phase, and λ_0 is a hyperangle-dependent asymptotic Sommerfeld parameter. The transition matrix $T_{\tilde{\mathbf{k}}_2, \tilde{\mathbf{k}}_3}$ that is built into the scattering solution can equivalently be defined as

$$T_{\tilde{\mathbf{k}}_2, \tilde{\mathbf{k}}_3} = \frac{4\pi}{q^2} \frac{1}{(2\pi)^3} \times \langle \Psi_{\tilde{\mathbf{k}}_2, \tilde{\mathbf{k}}_3}^-(\mathbf{r}_2, \mathbf{r}_3) | -Z + e^{i\mathbf{q} \cdot \mathbf{r}_2} + e^{i\mathbf{q} \cdot \mathbf{r}_3} | \Phi_i(\mathbf{r}_2, \mathbf{r}_3) \rangle, \quad (12)$$

which provides the more familiar expression used in the FBA. In our framework, the transition matrix is extracted from $\Phi_{sc}^+(\mathbf{q}, \mathbf{r}_2, \mathbf{r}_3)$, not from Eq. (12).

For two electrons escaping with energies E_2 and E_3 in the solid angles $d\Omega_2$ and $d\Omega_3$, the FDCS, within the FBA, is defined as

$$\frac{d^5\sigma}{d\Omega_2 d\Omega_3 d\Omega_f dE_2 dE_3} = (2\pi)^4 \frac{k_f k_2 k_3}{k_i} |T_{\tilde{\mathbf{k}}_2, \tilde{\mathbf{k}}_3}|^2, \quad (13)$$

where the projectile, whose energy $E_f = k_f^2/(2\mu_{TP})$ is determined by total-energy conservation, is scattered in the solid angle $d\Omega_f$. This definition allows for a direct comparison with experimental data. In order to compare our results with the theoretical results presented in Ref. [4,12], on the other hand, we shall also use the alternative, but equivalent, definition of the cross section

$$\frac{d\sigma}{d\mathbf{k}_2 d\mathbf{k}_3 d\mathbf{q}_\perp} = \frac{(2\pi)^4}{v_p^2} |T_{\tilde{\mathbf{k}}_2, \tilde{\mathbf{k}}_3}|^2, \quad (14)$$

which is differential with respect to the ejected electrons' momenta and the transverse momentum transfer \mathbf{q}_\perp (the perpendicular component of \mathbf{q} with respect to the beam axis); v_p is the velocity of the incident projectile.

We use the GSF method to solve the driven equation for a given \mathbf{q} . For convenience, as explained in [17,18], the helium ground state is also constructed within the GSF formalism. Negative energies of the GSF basis with negative energy were shown to be very efficient in obtaining two-electron bound states [22,32,33]. In order to calculate the scattering function, we proceed as outlined in Ref. [18]: $\Phi_{sc}^+(\mathbf{q}, \mathbf{r}_2, \mathbf{r}_3)$ is decomposed in total-angular-momentum partial waves and subsequently expanded in a Sturmian basis [see Eq. (19) of [18]]; this converts Eq. (10) into a linear system [similar to Eq. (21) of [18]] which is solved with standard methods. In all kinematical configurations considered below, convergence with respect to the number of partial waves has been verified. From $|\Phi_{sc}^+(\mathbf{q}, \mathbf{r}_2, \mathbf{r}_3)|$ at large enough ρ (50 a.u. for 20 eV excess energy and 120 a.u. for the low-energy configurations, 6 eV excess energy) we extract $|T_{\tilde{\mathbf{k}}_2, \tilde{\mathbf{k}}_3}|$ using Eq. (11) and, finally, the FDCS through either expression (13) or (14).

III. RESULTS

275

276 We arrange the results in three subsections. First, we
 277 compare our cross sections with the dynamically screened
 278 3C (hereinafter DS3C) and effective momenta 3C (hereinafter
 279 EM3C) results presented by López and coworkers [4,12]. The
 280 objective is twofold: (i) to evaluate which of the two analytic
 281 proposals is more appropriate and (ii) to provide results that
 282 can be used for numerical reference to test further perturbative
 283 models. We then explore the double-ionization dynamics for
 284 slow emitted electrons for both equal and unequal energy
 285 sharing and compare the outcome with the EM3C results. In
 286 this energy range, perturbative approaches are not appropriate
 287 but ours is, and we expect to explore the dominant processes
 288 within it. In the last subsection we compare our theoretical
 289 FDCS with available experimental data of Fischer *et al.* [11].

290 Only coplanar configurations are considered, and all angles
 291 are defined with respect to the incident-beam direction. The
 292 cross sections will be presented as contour plots in θ_2 and θ_3 ,
 293 with the intensity scale indicated on the right-hand side.

A. Comparison: GSF, DS3C, and EM3C

295 In order to compare our results with the work of López
 296 *et al.* [4,12], we consider here the double ionization of helium
 297 by protons impinging with an energy of 700 keV. Even in
 298 a first-order Born calculation, the use of effective charges
 299 allowed them to distinguish between positively and negatively
 300 charged projectiles. In our strictly FBA, no distinction can be
 301 made about the sign of the projectile. In Ref. [12], the authors
 302 presented, in a number of contour plots (and some selected
 303 cuts), the FDCS defined by Eq. (14). They showed that the
 304 results (shapes and magnitudes) are widely affected, on the
 305 one hand, by the representation of the initial target state and,
 306 on the other hand, by the effective charges chosen for the
 307 postcollisional dynamics.

308 Concerning the helium ground state employed, the one
 309 used in [4,12] and ours differ significantly. The authors
 310 of [12] use two types of Bonham and Kohl bound-state
 311 functions: a simple, two-parameter (type-7) function (called
 312 GS1) and a more refined, modified-type-9 one, with five
 313 parameters (called GS2). These trial functions yield bound
 314 energies of -2.8756 and -2.9019 a.u., respectively. In our
 315 formulation, the helium ground state is obtained with the GSF
 316 method [32,33], with an energy of -2.9033 a.u., using 20
 317 Sturmians per coordinate per partial wave, with individual
 318 angular momenta up to 4. In this paper we shall compare our
 319 cross-section results only with those of [4,12] that employ the
 320 GS2 ground state.

321 Since the main purpose of this contribution is to compare the
 322 descriptions of the continuum functions, in order to discard any
 323 initial-state-related issue, we have also considered a helium
 324 ground state of poorer quality, with an energy close to the
 325 GS2 counterpart (using as few as 5 Sturmians per partial
 326 wave per coordinate and keeping the same angular momentum
 327 values, we achieved a ground-state energy of -2.9024 a.u.).
 328 Both calculated FDCS presented no appreciable differences;
 329 therefore, we may consider that any discrepancy between the
 330 results of López *et al.* and ours is to be attributed essentially
 331 to the continuum functions.

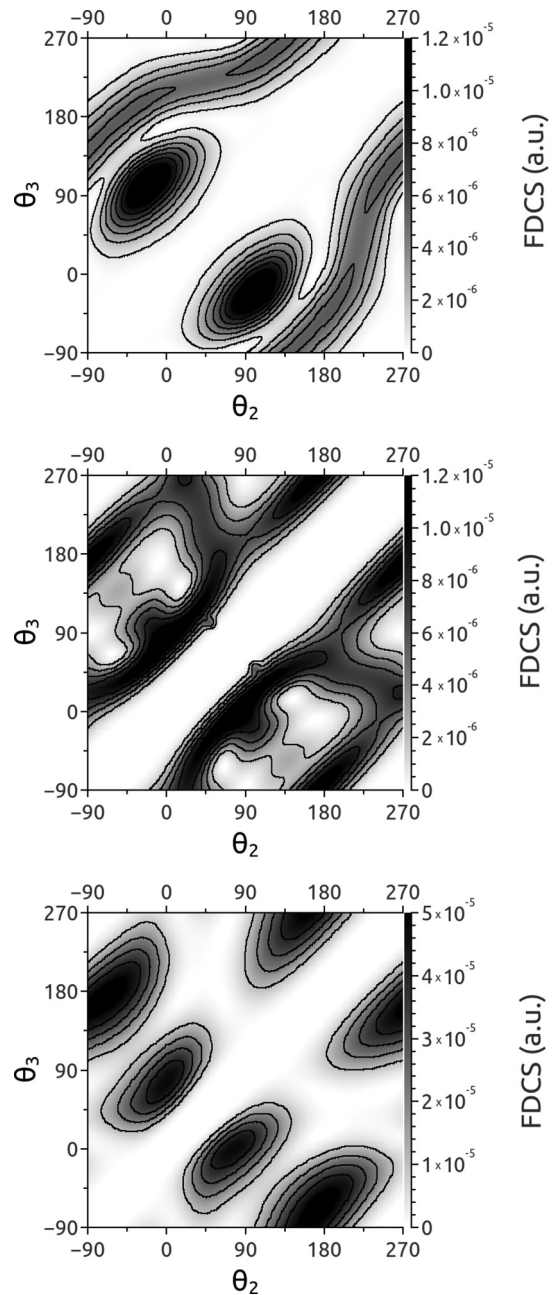


FIG. 1. Fully differential cross section for helium double ionization by proton impinging at 700 keV. The two emitted electrons each take 10 eV, and the proton transfers to the atomic system a momentum $q = 0.9$ a.u., oriented at $\theta_q = 40.18^\circ$. (top) Present GSF, (middle) DS3C [12], and (bottom) EM3C [4].

332 We start with the case in which the two electrons are ejected
 333 in the scattering plane in directions θ_2 and θ_3 with equal
 334 energy: $E_2 = E_3 = 10$ eV. This corresponds to a momentum
 335 transfer of modulus $q = 0.9$ a.u. oriented at $\theta_q = 40.18^\circ$. A
 336 comparison of results is presented by the contour plots in Fig. 1.
 337 The structures we obtain with the GSF method (top panel)
 338 differ substantially from the DS3C results [12] (middle panel).
 339 The GSF results vary less rapidly with the ejection angles.
 340 At the same time, the DS3C structures are more extended,
 341 in the sense that there is no clear frontier between the recoil

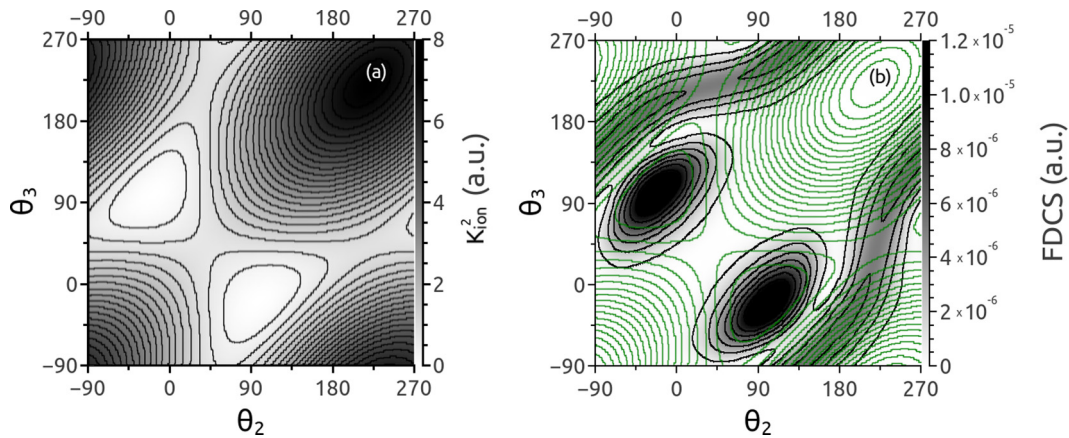


FIG. 2. (Color online) (a) Squared modulus of the momentum transferred to the helium nucleus K_{ion}^2 . Both electrons emerge equally sharing the 20 eV excess energy, $q = 0.9$ and $\theta_q = 40.18^\circ$ with respect to the incident direction. (b) GSF FDCS for these kinematical conditions, with the K_{ion}^2 contours superimposed [in green (gray)].

342 and the binary peaks. Less profound are the differences found
343 between the GSF and the EM3C [4] results (bottom panel).
344 They both present a smoother angular dependence but differ in
345 key features such as the recoil-structure shape and the relative
346 heights of each peak.

347 We should add here that, in the case of electron impact,
348 in contrast to the 3C counterpart, *ab initio* calculations
349 such as the convergent close coupling (CCC) [27] showed
350 a more prominent binary peak. In the present proton case, the
351 comparison between our numerical results and those of the 3C
352 variants reveals a similar feature.

353 There is also a subtle difference between the GSF result
354 and the 3C-based cross sections. As can be observed when
355 visually comparing Fig. 1 (top panel) with Fig. 2, the binary
356 peak location in the GSF case coincides exactly with a
357 configuration of minimum momentum transfer to the He^{++}
358 core, $\mathbf{K}_{\text{ion}} = \mathbf{q} - \mathbf{k}_2 - \mathbf{k}_3$. The peak is slightly displaced in the
359 DS3C and EM3C cross sections. Moreover, the DS3C model
360 binary peak occurs when the electrons are emitted at exactly
361 right angles. In our GSF calculation the binary peak appears
362 for electrons emitted at mutual angles that are wider than 90° ,
363 a feature readily explained by the interelectronic repulsion
364 forcing the fragments farther apart in coplanar geometry (the

same was also observed in other fully numerical results [16,27] 365
for double ionization by electron impact). 366

367 As a second comparison, consider now the same projectile
368 energy (700 keV), the same momentum transfer ($q = 0.9$ a.u.),
369 and the same excess energy (20 eV) but unequal energy
370 sharing: $E_2 = 5$ eV and $E_3 = 15$ eV. Our GSF and the DS3C
371 results of [12] are compared in Fig. 3. The binary peaks
372 are the most dominant features present in the GSF FDCS
373 for the unequal-energy example [see Fig. 3(a)]. The DS3C
374 scheme, in turn, appears to underestimate them (relative to
375 the binary and back-to-back structures), as shown in Fig. 3(b).
376 The DS3C approach presents back-to-back emission with the
377 faster electron ejected in the directions parallel or antiparallel
378 to the momentum transfer. Both situations are depicted as
379 equally likely in the DS3C FDCS. This is not the case in the
380 GSF result: only the emission of the faster electron in the
381 direction opposite to the momentum transfer is important [see
382 Fig. 3(a)].

383 The first likely candidate responsible for the back-to-back
384 structures, particularly with the fast electron emitted parallel
385 to \mathbf{q} , would be the shake-off mechanism. However, Dorn
386 *et al.* [34] ruled it out as a viable option to produce this
387 emission. They stated that the fast electron would have to be ejected

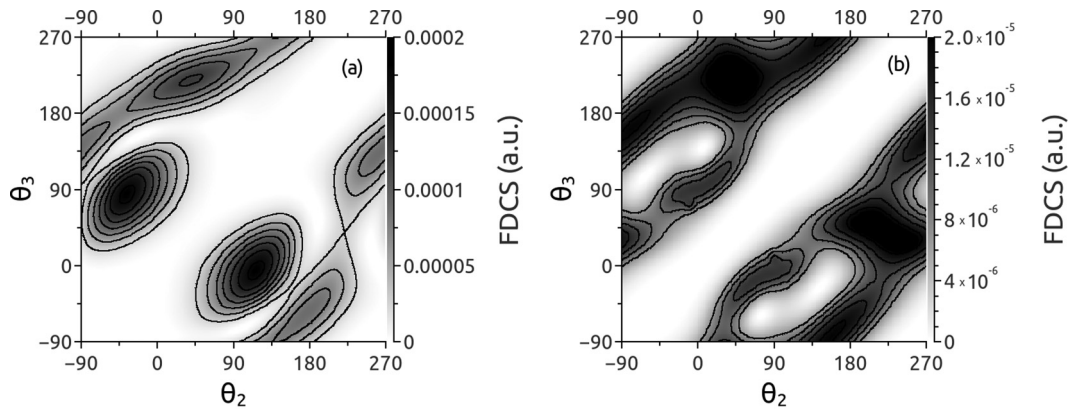


FIG. 3. Fully differential cross section for helium double ionization by protons impinging at 700 keV and transferring to the atomic system a momentum $q = 0.9$ a.u., oriented at $\theta_q = 40.18^\circ$. The two electrons are ejected with unequal energy sharing: $E_2 = 5$ eV, $E_3 = 15$ eV. (a) Present GSF and (b) DS3C [12].

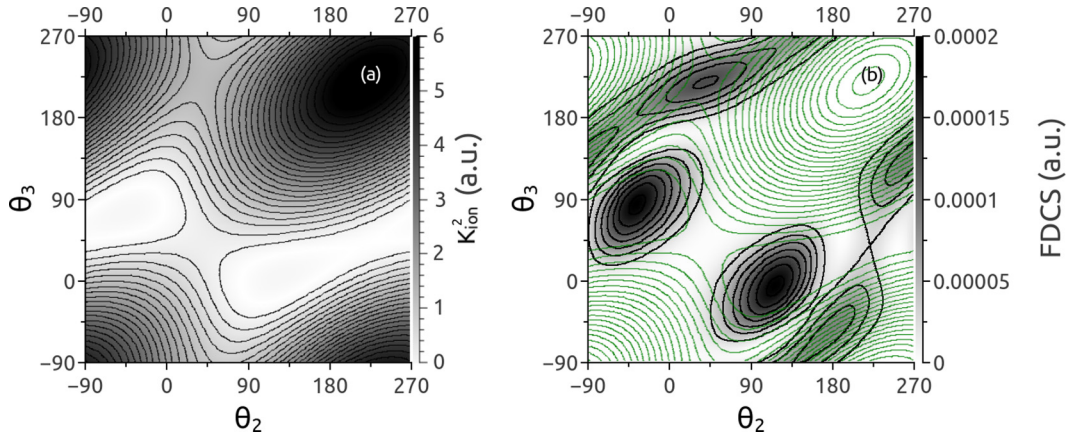


FIG. 4. (Color online) (a) Squared modulus of the momentum transferred to the nucleus K_{ion}^2 . (b) Same as Fig. 3(a), but superimposing the contours in (a) [in green (gray)].

388 with a higher velocity so that the effective charge change felt
 389 by the slow electron can be nonadiabatic. Therefore, for the
 390 energy sharing considered in this contribution, the mechanism
 391 can be disregarded. To explain the back-to-back peaks we are
 392 left with more abrupt mechanisms, involving pure collisions,
 393 and not soft relaxations to the continuum.

394 We now are going to briefly justify that the back-to-back
 395 emission, in our first-order Born context, should be dominant
 396 only when the fast electron leaves in the $-\mathbf{q}$ direction and
 397 weaker when it goes along \mathbf{q} . The occurrence is partly
 398 explained by Fig. 4. In Fig. 4(b) we show the GSF cross
 399 section superimposed with the contour plot of the squared
 400 modulus of the momentum transferred to the residual core
 401 [Fig. 4(a)]. After one of the electrons acquires the momentum
 402 provided by the projectile, the final back-to-back configuration
 403 requires at least one interaction with the nucleus; if that were
 404 not the case, there would be no electron (either of them) in
 405 the $-\mathbf{q}$ direction (indeed, a head-on collision of two bodies
 406 with equal mass would imply that they simply *swap* their
 407 respective momenta). The interaction with the core should
 408 transfer some momentum to the nucleus, with a magnitude
 409 of the order of the momentum of the electrons (i.e., on the
 410 order of 1). However, the final configuration with the fast
 411 electron parallel to \mathbf{q} gives nearly no momentum transfer to
 412 the nucleus and therefore is an unlikely process. The exactly

opposite scenario does incorporate an appreciable amount of
 momentum transferred to the core, denoting further intratarget
 interactions, and therefore cannot be ruled out. The above does
 not agree with the CCC (theoretical) FDCS presented in the
 work by Dorn *et al.* [34].

In contrast to the recoil and back-to-back structures, the
 binary ones do not require significant participation of the
 nucleus and therefore can exist in the (θ_2, θ_3) directions which
 imply almost no momentum acquired by the parent core [see
 Fig. 4(b)].

A second argument at play in the back-to-back phenomenon
 in Fig. 3 comes from the analysis of the driven term in Eq. (10).
 Retaining the dipolar term in the exponentials, we have

$$\begin{aligned} (Z - e^{i\mathbf{q}\cdot\mathbf{r}_2} - e^{i\mathbf{q}\cdot\mathbf{r}_3}) &\approx -i(\mathbf{q}\cdot\mathbf{r}_2 + \mathbf{q}\cdot\mathbf{r}_3) \\ &= -i\frac{\rho}{\kappa}\mathbf{q}\cdot(\tilde{\mathbf{k}}_2 + \tilde{\mathbf{k}}_3), \end{aligned} \quad (15)$$

where in the second approximation we used the position-
 dependent momenta $\tilde{\mathbf{k}}_j = \frac{\kappa}{\rho}\mathbf{r}_j$ ($j = 2, 3$), defined originally
 in [35] and more explicitly in [31]. In our formulation, it
 is the driven term that dictates how a particular geometrical
 configuration is enhanced or suppressed (see [18]). We thus
 plot in Figs. 5(a) and 5(b) the magnitude $|\hat{\mathbf{q}}\cdot(\tilde{\mathbf{k}}_2 + \tilde{\mathbf{k}}_3)|$ and a
 superimposition with the FDCS, respectively. This comparison
 is in line with the electron-impact analysis presented by

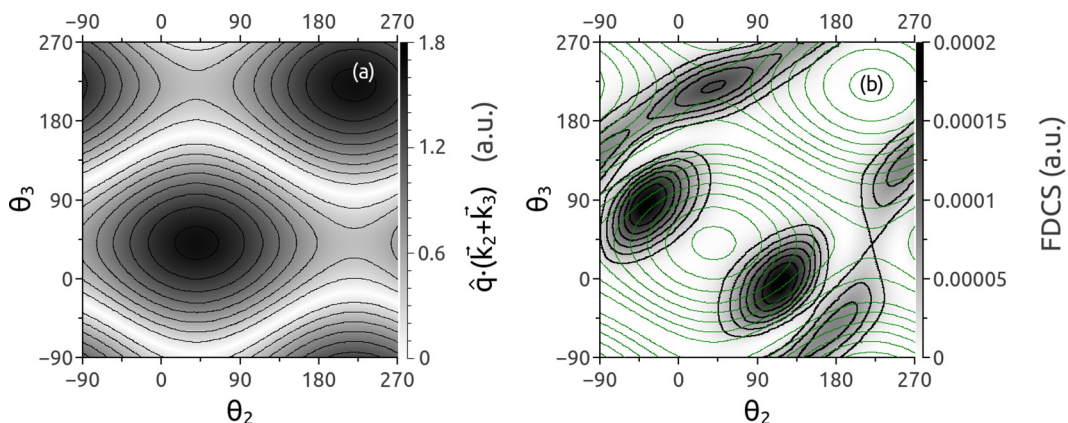


FIG. 5. (Color online) (a) $|\hat{\mathbf{q}}\cdot(\tilde{\mathbf{k}}_2 + \tilde{\mathbf{k}}_3)|$. (b) Same as Fig. 3(a), but superimposing the contours in (a) [in green (gray)].

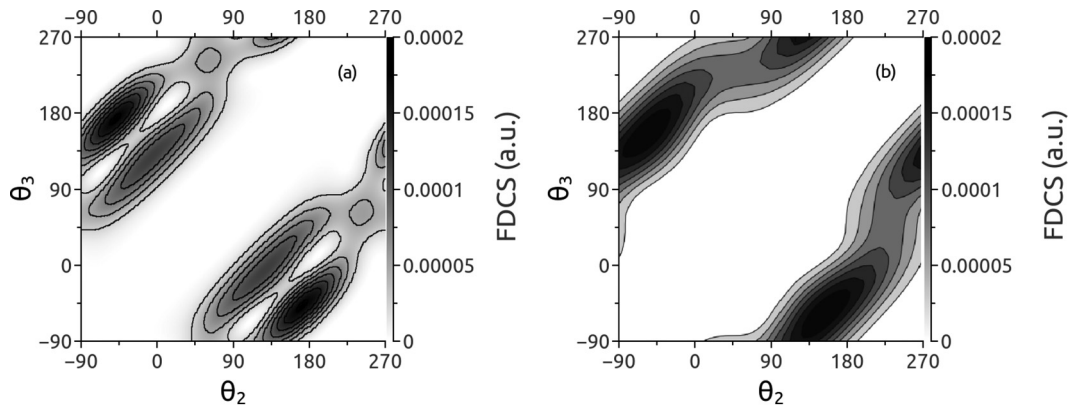


FIG. 6. Fully differential cross section for helium double ionization by protons impinging at 700 keV and transferring to the atomic system a momentum $q = 0.9$ a.u., oriented at $\theta_q = 40.18^\circ$. The two ejected electrons both have 3 eV. (a) Present GSF and (b) EM3C [4].

434 Lahmam-Bennani *et al.* [14], who related the dips in the FDCS
435 considering the conditions that nullify Eq. (15).

436 The introduction of effective charges into the 3C function
437 is a means to account for the interactions between the target
438 components as well as the projectile with the target subsystem.
439 The charges affect very strongly the shapes and magnitudes
440 of the corresponding FDCS, as can be seen in the systematic
441 3C versus DS3C comparison in [12]. The dynamical screening
442 corrects the 3C overestimation of the back-to-back emission
443 but introduces rapidly varying structures that cannot be
444 reproduced in our *ab initio* calculation. Thus, we infer that the
445 use of such approximate analytical three-body functions leads
446 to results that are not without shortcomings. We should add that
447 there exists a large variety of effective-charge proposals, and
448 there is not a clear way to choose which one is the appropriate.
449 So it is difficult to be certain about the correctness of the
450 obtained results.

451 B. Low-ejected-energy regime

452 We now consider the regime of two electrons ejected at
453 lower energies. The application of distorted-wave methods
454 to this emission regime can be seen as an overreach, but
455 nonetheless, we will see that the EM3C approach can manage
456 to describe some key FDCS features. In Ref. [4] the authors
457 evaluated the double ionization of helium by proton (and
458 antiproton) impact, ejecting the electrons at slow velocities.
459 Their equal emission energies are 3 eV, with $q = 0.9$ a.u.
460 oriented at $\theta_q = 40.18^\circ$ and an incident energy of 700 keV
461 for the protonic projectiles. Our exact treatment of the two-
462 electron continuum enables us to explore confidently this low-
463 energy situation and provides insight that is complementary to
464 that performed by López and coworkers using distorted-wave
465 methods. In Fig. 6 we compare our GSF result with the
466 EM3C one [4]. Both approaches indicate a recoil peak more
467 relevant than the binary one. This can be understood since
468 the electrons acquire small velocities after the collision and
469 they may interact one further time with the core. The classical
470 picture corresponds to an orbit around the nucleus before the
471 electron is finally released.

472 While the EM3C results suggest a disappearance of the
473 binary peak, the same is not observed in our GSF FDCS, which

474 presents a diminished but still present binary peak. Although
475 not exactly matching our *ab initio* results, the EM3C manages
476 to give a qualitative agreement that reflects the most significant
477 cross-section structure, namely, the recoil peak. This is a strong
478 hint that the effective momentum approach makes possible the
479 application of distorted-wave approximations within energy
480 ranges that would normally be regarded as inappropriate.

481 Still within the low-ejected-energy regime, another kine-
482 matical condition was considered: a momentum transfer above
483 unity to allow for more nondipolar effects: $q = 1.25$ a.u.,
484 oriented at $\theta_q = 61.82^\circ$, with a projectile energy maintained
485 at 700 keV with an excess energy of 6 eV. Equal- and unequal-
486 energy-sharing conditions are studied, with both electrons
487 emitted with 3 eV or (1.5 + 4.5) eV. The amount of momentum
488 transfer to the target would indicate some expected back-to-
489 back emission. This is indeed confirmed by observing both
490 equal- and unequal-energy-sharing configurations in Fig. 7,
491 with the effect being more dominant in the latter.

492 For the equal-energy-sharing scenario [Fig. 7(a)] we have
493 again recoil structures which are higher than the binary ones.
494 In comparison to Fig. 6, the main differences that emerge are
495 the slightly more pronounced back-to-back emission and a
496 stronger binary peak.

497 The unequal-energy case, as in Sec. III A, shows back-to-
498 back emission when the fast electron goes against the direction
499 of the momentum transfer. The slower electron is pushed
500 preferentially in the \mathbf{q} direction, with their mutual repulsion
501 serving as a guide. Under this particular kinematical condition,
502 there is a large amount of momentum transferred to the target,
503 yet the electrons leave with slow velocities. Therefore, the core
504 has to absorb a portion of that transferred momentum in most
505 emission geometries. Regarding the back-to-back ejection, we
506 observe the same result as in the previous section: it is more
507 likely to have the fast electron sent in the $-\mathbf{q}$ direction. Both
508 arguments apply, but in the present case the dipolar terms of the
509 exponential yield a near-zero value that is nearly replicated in
510 the FDCS; Fig. 8 shows a comparison similar to that in Fig. 5.

511 As can be expected, recoil and binary peaks imply ejections
512 at narrower mutual angles when the energy is shared evenly.
513 This configuration maximizes the velocity magnitude sum and
514 roughly implies that the electrons have less interaction time to
515 push each other apart.

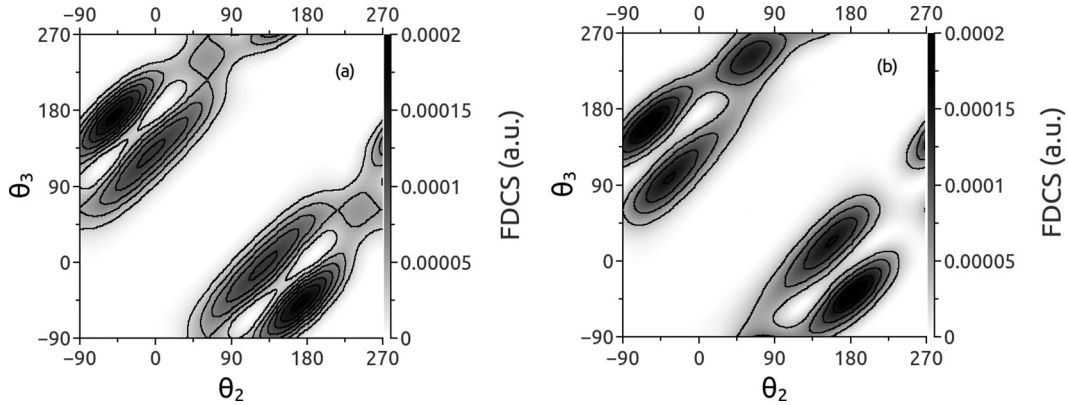


FIG. 7. GSF fully differential cross section for helium double ionization by protons impinging at 700 keV and transferring to the atomic system a momentum $q = 1.25$ a.u., oriented at $\theta_q = 61.82^\circ$. The excess energy E_a is 6 eV. (a) Equal energy sharing $E_2 = E_3 = 3$ eV. (b) Unequal energy sharing, $E_2 = 1.5$ eV, $E_3 = 4.5$ eV.

C. Comparison with experimental data

516

517 So far, we have looked at several physical aspects, compar-
 518 ing our GSF results with those of López and collaborators.
 519 In this section we compare our calculations with the data
 520 set (relative scale) measured by Fischer *et al.* [11]. In their
 521 experiment, the incident proton has an energy of 6 MeV,
 522 considerably faster than those studied in the previous sections.
 523 Due to the low experimental counting rate, the measurements
 524 were made with the collection of electrons with $E_2 = E_3 <$
 525 25 eV and momentum transfers ranging in magnitude q from
 526 1.4 to 2.0 a.u and in angle θ_q from 75° to 85° . This range of
 527 variation for the quantities E_2, E_3, \mathbf{q} implies that the label *fully*
 528 *differential* applies loosely for the measured cross sections.
 529 The most critical variable is the variation of q since the FDCS
 530 inherits an explicit factor $1/q^4$. Therefore, we considered an
 531 average q value using the following expression:

$$\langle q \rangle = \left[\frac{1}{q_{\max} - q_{\min}} \int_{q_{\min}}^{q_{\max}} \frac{1}{q^4} dq \right]^{-1/4}, \quad (16)$$

532 which for $q_{\min} = 1.4$ a.u. and $q_{\max} = 2.0$ a.u. yields $\langle q \rangle =$
 533 1.656 a.u. For the direction of the momentum transfer, we took
 534 the intermediate value $\theta_q = 80^\circ$. The total emission energy
 535 considered in our calculation was also chosen in the middle of
 536 the measured range: 10 eV per electron.

537 The cross sections, as defined by Eq. (13), are presented in
 538 Fig. 9. Our GSF calculation (contour plots, top panel) are compared
 539 with experimental data (middle panel). To appreciate the
 540 qualitative agreement between them, we present in the bottom
 541 panel a superposition of both results. In the small- q regime,
 542 the back-to-back configuration is not favored like the dipolar
 543 behavior observed with electron-impact collisions [14]. As
 544 the momentum transfer is increased, nondipolar terms become
 545 relevant: indeed, we observe in the calculated FDCS an
 546 important amount of back-to-back emission, and the binary
 547 and recoil peaks have very different shapes. The results show
 548 a strong, localized, binary peak; the recoil peak, in contrast,
 549 merges with the back-to-back one, forming a *wall* that has a dip
 550 in height precisely where the first-order Born symmetry axis
 551 crosses it. Unfortunately, the experimental detector range [11]
 552 precludes a comparison in the region where the recoil and
 553 back-to-back wall gains height.

554 An aspect that emerges from Fig. 9(b) is the small number
 555 of counts in the experiment. It does still allow for the visual-
 556 ization of some structures, but they are less clearly delimited
 557 than in previous electron-impact experiments from the same
 558 group [16,34,36]. This small number of counts, sadly, does
 559 not allow us to make a more detailed comparison. A higher
 560 impact count could result in more reliable and descriptive
 561 experimental cross sections, which in turn would call for a

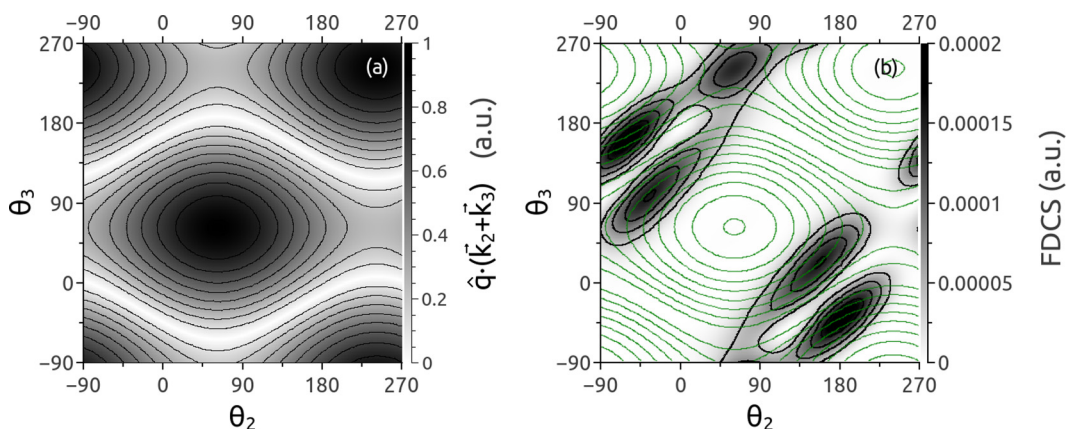


FIG. 8. (Color online) (a) $|\hat{\mathbf{q}} \cdot (\tilde{\mathbf{k}}_2 + \tilde{\mathbf{k}}_3)|$. (b) Same as Fig. 7(a), but superimposing the contours in (a) [in green (gray)].

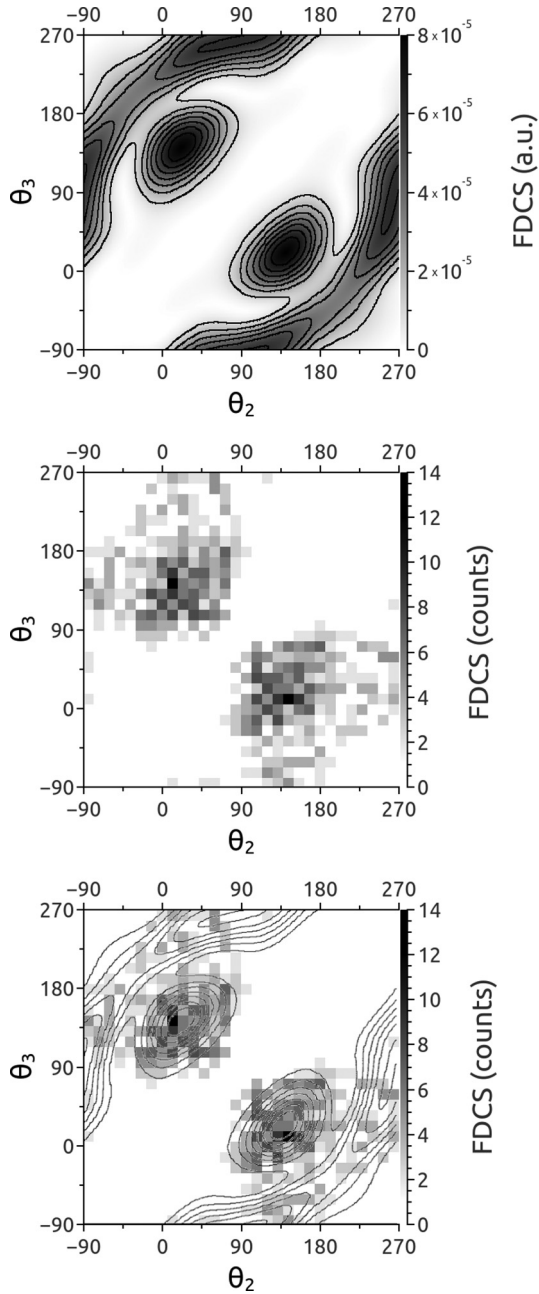


FIG. 9. Fully differential cross section for helium double ionization by protons impinging at 6 MeV, with two electrons ejected with the same energy. (top) Present GSF with momentum transfer $q = 1.65$, oriented at $\theta_q = 80^\circ$ and $E_2 = E_3 = 10$ eV. (middle) Relative experimental data [11] with a momentum transfer in the range $q = 1.4\text{--}2.0$ a.u., oriented in between $\theta_q = 75^\circ$ and 85° and $E_2 = E_3 < 25$ eV. (bottom) Superposition of the theoretical and experimental cross sections.

more sophisticated calculation with an actual integration on the energies and transferred momenta ranges, be it analytical or entirely numerical. This said, we may state that there is fair theory-experiment agreement in the cross-section shapes.

IV. SUMMARY

In the present contribution we have investigated FDCS for the double ionization of helium by protonic impact in different

kinematical configurations. We tackled the problem within a first Born approximation frame regarding the projectile-target interaction and employing the generalized-Sturmian-function method to solve in a numerically exact way the resulting three-body continuum problem.

Our *ab initio* results allowed us to test the validity of approximate analytical double-continuum wave functions with effective charges or effective momenta. With the comparison in the explored kinematical conditions, we can state that (i) none of these schemes can provide an exact agreement with our calculations and (ii) of the two, the effective momentum approach can be deemed more physically plausible since it yielded FDCS which vary less abruptly with the ejection angles, similar to what was observed in our numerical results.

The EM3C approach has also been applied within a low-emission-energy regime [4]. Being slowly ejected, the electrons have time to interact with each other and with the core many times, corresponding to high orders in a multiple-scattering series [2]. These interactions are solved to every order by our *ab initio* GSF methodology. Although perturbative methods are normally considered not well suited to describe the dynamics of slowly ejected electrons, the EM3C model surprisingly managed to characterize the most dominant cross-section feature, namely, the recoil peak. While it still missed the binary and back-to-back contributions that show up in our GSF calculation in the $(3 + 3)$ eV regime, the study indicates that the EM3C provided an interesting step forwards for perturbative approaches.

The final results section was devoted to a theory-experiment FDCS comparison. We calculated GSF cross sections, attempting to replicate the relative experimental data of Fischer *et al.* [11], who registered low counting rates. Globally, we observed fair qualitative agreement, in particular with respect to two key features: the location of the maximum corresponding to the binary peak and the presence of a dip where the recoil peak was expected. There is also an experimental hint of a local peak in the cross section, corresponding to our theoretical back-to-back peak, but this falls outside of the detection angles for the cold-target recoil-ion momentum spectroscopy apparatus [11].

New fully differential experimental data, with fast incident protons, would be very welcome in order to validate the benchmark cross sections presented here. Furthermore, as was done with electron-impact ionization [13,15,16,37], the incidence energy could be lowered to quantify the appearance of second-order Born effects. We hope that our contribution will help with further theoretical developments in improving perturbation schemes.

ACKNOWLEDGMENTS

We thank Dr. S. D. López and Dr. D. Fischer for providing the results of their previous publications in tabular form. We acknowledge the support from PIP 201301/607 CONICET (Argentina), and one of the authors (G.G.) is also thankful for the support from PGI 24/F059 of the Universidad Nacional del Sur. We acknowledge the CNRS (PICS 06304) and CONICET (Project No. DI 158114) for funding our French-Argentinean collaboration.

- [1] L. Gulyás, A. Igarashi, and T. Kirchner, *Phys. Rev. A* **86**, 024701 (2012).
- [2] J. Berakdar, A. Lahmam-Bennani, and C. Dal Cappello, *Phys. Rep.* **374**, 91 (2003).
- [3] M. Schulz, M. F. Ciappina, T. Kirchner, D. Fischer, R. Moshhammer, and J. Ullrich, *Phys. Rev. A* **79**, 042708 (2009).
- [4] S. D. López, S. Otranto, and C. R. Garibotti, *Phys. Rev. A* **87**, 022705 (2013).
- [5] M. B. Shah and H. B. Gilbody, *J. Phys. B* **18**, 899 (1985).
- [6] L. H. Andersen, P. Hvelplund, H. Knudsen, S. P. Møller, K. Elsener, K. G. Rensfelt, and E. Uggerhøj, *Phys. Rev. Lett.* **57**, 2147 (1986).
- [7] L. H. Andersen, P. Hvelplund, H. Knudsen, S. P. Møller, J. O. P. Pedersen, S. Tang-Petersen, E. Uggerhøj, K. Elsener, and E. Morenzoni, *Phys. Rev. A* **41**, 6536 (1990).
- [8] M. Schulz, R. Moshhammer, W. Schmitt, H. Kollmus, B. Feuerstein, R. Mann, S. Hagmann, and J. Ullrich, *Phys. Rev. Lett.* **84**, 863 (2000).
- [9] M. Foster, J. Colgan, and M. S. Pindzola, *Phys. Rev. Lett.* **100**, 033201 (2008).
- [10] X. Guan and K. Bartschat, *Phys. Rev. Lett.* **103**, 213201 (2009).
- [11] D. Fischer, R. Moshhammer, A. Dorn, J. R. Crespo López-Urrutia, B. Feuerstein, C. Höhr, C. D. Schröter, S. Hagmann, H. Kollmus, R. Mann *et al.*, *Phys. Rev. Lett.* **90**, 243201 (2003).
- [12] S. D. López, C. R. Garibotti, and S. Otranto, *Phys. Rev. A* **83**, 062702 (2011).
- [13] A. Kheifets, I. Bray, Lahmam-Bennani, A. Duguet, and I. Taouil, *J. Phys. B* **32**, 5047 (1999).
- [14] A. Lahmam-Bennani, I. Taouil, A. Duguet, M. Lecas, L. Avaldi, and J. Berakdar, *Phys. Rev. A* **59**, 3548 (1999).
- [15] A. Lahmam-Bennani, A. Duguet, M. N. Gaboriaud, I. Taouil, M. Lecas, A. Kheifets, J. Berakdar, and C. D. Cappello, *J. Phys. B* **34**, 3073 (2001).
- [16] A. Dorn, A. Kheifets, C. D. Schröter, B. Najjari, C. Höhr, R. Moshhammer, and J. Ullrich, *Phys. Rev. Lett.* **86**, 3755 (2001).
- [17] M. J. Ambrosio, F. D. Colavecchia, D. M. Mitnik, and G. Gasaneo, *Phys. Rev. A* **91**, 012704 (2015).
- [18] M. J. Ambrosio, F. D. Colavecchia, G. Gasaneo, D. M. Mitnik, and L. U. Ancarani, *J. Phys. B* **48**, 055204 (2015).
- [19] I. Bray, *Phys. Rev. Lett.* **89**, 273201 (2002).
- [20] C. W. McCurdy, M. Baertschy, and T. N. Rescigno, *J. Phys. B* **37**, R137 (2004).
- [21] M. Silenou Mengoue, M. G. Kwato Njock, B. Piraux, Y. V. Popov, and S. A. Zaytsev, *Phys. Rev. A* **83**, 052708 (2011).
- [22] G. Gasaneo, L. U. Ancarani, D. M. Mitnik, J. M. Randazzo, A. L. Frapiccini, and F. D. Colavecchia, *Adv. Quantum Chem.* **67**, 153 (2013).
- [23] C. R. Garibotti and J. E. Miraglia, *Phys. Rev. A* **21**, 572 (1980).
- [24] J. S. B. M Brauner and H. Klar, *J. Phys. B* **22**, 2265 (1989).
- [25] D. M. Mitnik, F. D. Colavecchia, G. Gasaneo, and J. M. Randazzo, *Comput. Phys. Commun.* **182**, 1145 (2011).
- [26] J. M. Randazzo, D. M. Mitnik, G. Gasaneo, L. U. Ancarani, and F. Colavecchia, *Eur. J. Phys. D* **69**, 189 (2015).
- [27] A. S. Kheifets, I. Bray, J. Berakdar, and C. Dal Cappello, *J. Phys. B* **35**, L15 (2002).
- [28] S. D. López, S. Otranto, and C. R. Garibotti, *Phys. Rev. A* **89**, 062709 (2014).
- [29] M. F. Ciappina, T. Kirchner, and M. Schulz, *Phys. Rev. A* **84**, 034701 (2011).
- [30] G. Gasaneo, D. M. Mitnik, J. M. Randazzo, L. U. Ancarani, and F. D. Colavecchia, *Phys. Rev. A* **87**, 042707 (2013).
- [31] A. S. Kadyrov, A. M. Mukhamedzhanov, A. T. Stelbovics, I. Bray, and F. Pirlepesov, *Phys. Rev. A* **68**, 022703 (2003).
- [32] J. M. Randazzo, A. L. Frapiccini, F. D. Colavecchia, and G. Gasaneo, *Phys. Rev. A* **79**, 022507 (2009).
- [33] J. M. Randazzo, A. L. Frapiccini, F. D. Colavecchia, and G. Gasaneo, *Int. J. Quantum Chem.* **109**, 125 (2009).
- [34] A. Dorn, A. Kheifets, C. D. Schröter, B. Najjari, C. Höhr, R. Moshhammer, and J. Ullrich, *Phys. Rev. A* **65**, 032709 (2002).
- [35] E. O. Alt and A. M. Mukhamedzhanov, *Phys. Rev. A* **47**, 2004 (1993).
- [36] A. Dorn, G. Sakhelashvili, C. Höhr, A. Kheifets, J. Lower, B. Najjari, C. Schröter, R. Moshhammer, and J. Ullrich, in *Electron and Photon Impact Ionization and Related Topics, IOP Conference Proceedings Vol. 172* (2003), p. 41.
- [37] A. Lahmam-Bennani, E. M. S. Casagrande, A. Naja, C. D. Cappello, and P. Bolognesi, *J. Phys. B* **43**, 105201 (2010).